IEEE Photonics Journal
An IEEE Photonics Society Publication

Open Access

Rapid fabrication of Spiral Varying Retarder for Using in Simple Schemes of Generating Radial and Azimuthal Vector Optical Fields

Volume 11, Number 5, October 2019

Victoria Shkuratova
Galina Kostyuk
Maksim Sergeev
Elena Vikhrova

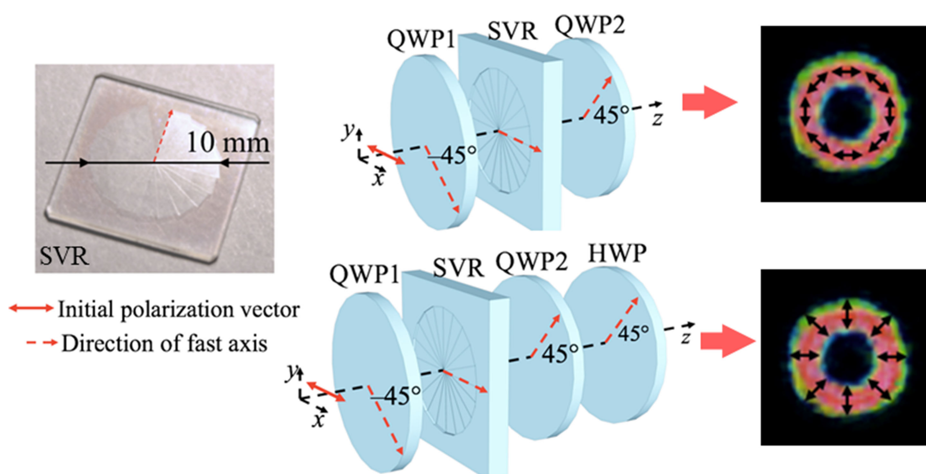

DOI: 10.1109/JPHOT.2019.2934761

IEEE photonics SOCIETY
IEEE

Rapid fabrication of Spiral Varying Retarder for Using in Simple Schemes of Generating Radial and Azimuthal Vector Optical Fields

Victoria Shkuratova, Galina Kostyuk, Maksim Sergeev, and Elena Vikhrova

ITMO University, Sankt -Petersburg 197101, Russia

DOI:10.1109/JPHOT.2019.2934761
This work is licensed under a Creative Commons Attribution 4.0 License. For more information, see https://creativecommons.org/licenses/by/4.0/

Manuscript received May 3, 2019; revised July 31, 2019; accepted August 7, 2019. Date of publication August 12, 2019; date of current version August 23, 2019. This work was supported by the Ministry of Education and Science of the Russian Federation under research agreement 14.587.21.0037 (RFMEFI58717X0037). Corresponding author: Victoria Shkuratova (e-mail: shkuratova_va@mail.ru).

Abstract: In this paper, the simple, reliable and efficient fabrication technology of spiral varying retarder (SVR) on Iceland spar for generating radially and azimuthally polarized beams from linearly polarized Gaussian beam for $\lambda = 632.8$ nm is shown. The SVR which consists of 20 sectors was made by laser-induced microplasma processing on plate area of 10×10 mm^2 in less than 7 minutes. When placing the SVR between two quarter wave plates with orthogonal fast axes the registration of typical images of intensity distribution in the far field in four analyzer positions (0°, 45°, 90°, 135°) confirmed the SVR's ability to generate radially polarized vector optical field. It was also shown that the placing of a half-wave plate, the fast axis of which is oriented at 45° relative to the direction of *x* axis, allows to create an azimuthally polarized vector optical field.

Index Terms: Optical device fabrication, crystalline materials, birefringence, optical retarders optical polarization, vector optical fields, materials processing, plasma etching.

1. Introduction

In recent years radially and azimuthally polarized light with cylindrical polarization symmetry is widely used in the large amount of high technology applications like optical trapping [1], [2], cooling of atoms [3], super-resolution microscopy [4], including localized surface plasmon microscopy [5], as well as data record and shortage systems [6]. It can also be used to improve the microprocessing quality in laser technology [7]–[11].

For generation of the radially and azimuthally polarized beams with annular shape it was suggested substantial number of optical elements (OEs) and units placed inside or outside the cavity. Mostly in reported methods the generation of radially and azimuthally polarized light provides placing a specially constructed OE inside the cavity [12]–[14]. However, it leads to additional losses, also makes constructing of laser not only difficult, but impossible in some cases, for example, when constructing high power fiber lasers. It is for this reason placing of OE outside the cavity seems to be less complex in implementation and more attractive, especially for the example, mentioned above. Polarization converters can de designed for incident beam with linear and circular polarization.

For the incident linearly polarized beam an half wave plate (HWP) with continuously varying fast axis direction has to be constructed, with rotates the incident linear polarization by the angle necessary to produce a radial distribution of the electric field [9], [15], [16]. The azimuthal distribution of the electric field will be observed at HWP's output by its rotation by 45° [15]. The disadvantage of this simplest device for generating a radially or azimuthally polarized electric field distribution is its fabrication technology, which consists in fabrication of segments with different orientations of the direction of the fast axis and further fixing them with glue on a glass substrate or fused silica. Obviously, the presence of glue between the sectors and the substrate in such devices makes them unacceptable for the conversion of high-power laser beams. Also, subwavelength grating, generating local HWPs, can be used for generation of radially and azimuthally polarized light [17]. Such OEs alone translate linearly polarized light into radially polarized light and are also characterized by high radiation and thermal stability when formed on fused silica. However, their fabrication requires the recording of very deep structures with high resolution, for which a long and multistage process of electron-beam lithography is used [17].

Much more devices and schemes are proposed for conversion of the incident circularly polarized beam. The radial or azimuthal polarization can be formed with a space-variant quarter wave plate (QWPs) possessing a radial symmetry [18]. Devices of QWPs are currently fabricated by the traditional method of creating sectors with different orientation of the fast axis and their further fixation using glue on glass plates or fused silica. Obviously, such devices also have a low damage threshold. Recently there have been reports of using self-assembled nanostructures, working like the space-variant QWPs, to convert circularly polarized Gaussian beams [19], [20]. They are made on amorphous materials with high damage threshold by direct femtosecond laser recording. The fabrication duration of such OEs for areas with a size of 1.2 mm with nanostructures is 1.5 hours [19]. From the description of the resulting vector optical field at the output of QWPs with radial symmetry, the corresponding Jones vector shows that when the left circular polarized light vector falls on QWPs, the resulting vector optical field corresponds to the distribution of the azimuthal vector optical field with orbital angular momentum $l = 1$. When the right circular polarized light vector falls on QWPs the right of circularly polarized light, described by the corresponding Jones vector, at its output, the resulting vector optical field is characterized by radial distribution with $l = -1$ [19].

The use of polarization converter schemes based on spatial light modulators (SLM) [21], [22], as also described above segmented HWPs [15] and segmented QWPs [23] is limited to the application with only low power lasers. This is due to their low destruction threshold. The schemes based on the use of diffraction-phase elements [24], spiral phase plate (SPP), operating in conjunction with a linear analyzer of the radial type [25], and elements whose operation principle based on electro-optical induced birefringence [26], are difficult to adjust due to the high sensitivity of these elements to mechanical displacements. The use of interference methods [27], including the placement of the SPP in one of the arms of the interferometer [28], are characterized by an even higher sensitivity to mechanical displacements than those listed earlier.

Consideration of the various elements and units used to create a radially polarized vector optical field made it possible to establish that the value of such devices will increase multiply, if they are sufficiently simple additional OE (or OEs) will allow to create an azimuthally polarized vector optical field. At the same time, an additional OEs will be relatively simple to fabricate and alignment, as well as schemes with their use will be built on a single optical path.

The consideration outlined above did not include the creation of arbitrary vector optical fields associated with the use of metasurfaces, which can significantly improve and simplify the schemes for their implementing [23], [29], [30]. This is due to the fact that the creation of meta-surfaces and basis of the principles of their work is based on approaches that are currently at the stage of scientific research.

The promising direction of solving the problem of conversion high power linearly polarized Gaussian beams into annular beams with radial polarization is relatively easy in implementation using of unit consisting of two QWPs and SVR, made on a plate of linear birefringent uniaxial crystal, whose crystal axis is parallel to the plate's surface (Y-cut). The principle of operation of

such SVRs is considered in detail, analyzed and experimentally confirmed in Refs. [31], [32]. Also, SVR's design can be summarized as follows. SVR is an OE divided into sectors with a spiral-like relief h_{SVR}, varying with azimuth angle θ in accordance with the expression [31]:

$$h_{SVR} = h_0 - \frac{\lambda\theta}{\pi\,|n_o - n_e|}; \quad h_0 = \frac{m\lambda}{|n_o - n_e|}, \tag{1}$$

where h_0 is the initial crystal thickness ($\theta = 0°$), λ is the wavelength, n_o and n_e are the refractive indices for ordinary and extraordinary waves respectively, m is an integer, θ varies within 0 to 2π.

For conversion of linearly polarized light firstly into circularly polarized and then into radially polarized light, the SVR was placed between two orthogonally oriented QWPs, wherein slow axis of the first QWP was oriented at 45° to the x axis direction, and the slow axis of SVR was oriented at 45° to the x axis direction [32].

At present time, as far as we know, two fabrication technologies were used to make such birefringent plates [31], [32]. The first one was based on laser-induced backside wet etching (LIBWE) and was used to fabricate SVR on crystalline quartz – the material most commonly used in polarization optics owing to its exceptionally low losses in a wide spectral range (0.15 – 4.50 μm). The quality of a radially polarized beam generating by SVR produced in accordance with the LIBWE technology on a Y-cut of crystalline quartz turned out to be low. According to the authors' opinion of Ref. [32], this was directly related to the choice of the SVR fabrication technology. They also proposed SVR fabrication technology based on the use of a multistage dry etching process with inductively coupled argon gas plasma using silicone masks, the number of which was determined depending on the number of SVR sectors [32]. For SVRs from 8 sectors, 7 masks were used, that is, one less than the number of sectors. It was shown in Ref. [32] that for the conversion of linearly polarized light into radially polarized with an error in the phase shift of less than 5%, it is necessary to include at least 8 sectors in the SVR. The thickness of the first sector was considered to be equal to the thickness of the crystal plate from an uniaxial negative α-BBO crystal, which has significant birefringence in the range of its high transparency (0.19 – 3.50 μm). The etching depth of each sectors provided that the value of the azimuth angle θ depends on the consecutive number of the sector as $2(s-1)\pi/S$, was calculated as follows [32]:

$$h = h_0 - h_{SVR} = \frac{2\lambda\,(s-1)}{S\,|n_o - n_e|}, \tag{2}$$

where s is the consecutive number of sector, S is general number of sectors.

Testing the eight-sector SVR by placing it between two QWPs, despite a slight deviation in the thickness of each sector from the calculated ones, showed the purity of the detected radial polarization, close to the theoretical maximum possible for SVR with 8 sectors [32]. According to the concept of work performed by SVR, when converting of a linearly polarized beam into a radially polarized beam, an increase in the number of sectors would imply a higher purity of the polarization state [31], [32]. When using etching with silicone masks an increase in the number of sectors will not lead to an increase in the duration of etching, since it is determined by the total depth of etching for a given wavelength. However, an increase in the number of sectors will certainly complicate the process of positioning, centering the masks relative to the fast axis of the crystal plate and their removal upon complexity of the etching process for each of sectors, and thus lead to a significant increase in the duration of SVR fabrication under this technology.

For the SVR's fabrication can be used gray scale photolithography with subsequent ion etching. Despite its high quality such technology is a long multi-step process requiring high precision facilities. Today gray-scale photolithography is already used for fabrication a birefringent phase plate (BPP) on YVO_4 crystal [33]. The BPP operates in conjunction with a polarization demodulator consisting of a QWP, the fast axis of which is oriented at 22.5° to the x axis direction and an HWP, the fast axis of which is oriented at 45° to the x axis direction [33]. This placing allows to generate arbitrary polarized vector optical field. The principle of BPP operation shows that using a BPP of continuous profile with a demodulator allows creating arbitrary vector optical fields. To confirm the ability of BPP in conjunction with QWP and HWP to create an arbitrary vector optical field, the distribution of

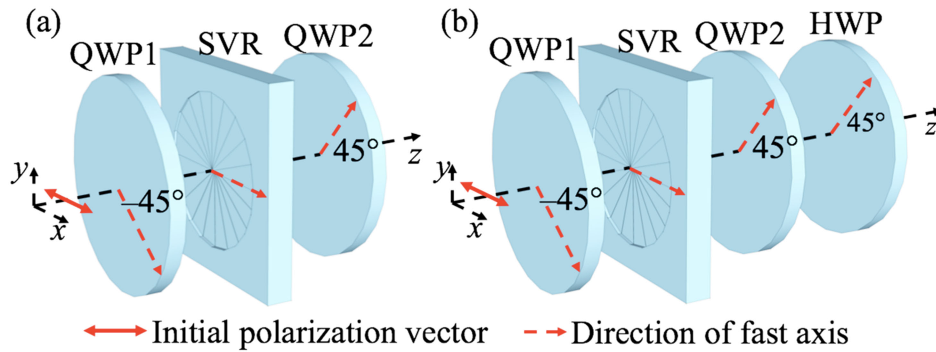

Fig. 1. Optical schemes for conversion of a linearly polarized beam: (a) into light with radial polarization; (b) with azimuthal polarization.

the BPP etching depth for the implementation of the radial vector optical field was calculated and constructed and tested according to the BPP calculation [33]. Experimental results were consistent with numerical simulations with insignificant different due to manufacturing errors. The BPP, like SVR, is set to a single optical path, and its principle of operation is close to the principle of the SVR.

So, the SVR is a relatively simple and convenient in operation OE that can transform linearly polarized Gaussian beams into annular beams with high quality radial polarization in combination with two QWPs. We suppose that SVR has not been widely used yet because lack of simple, reliable and efficient technology of its fabrication on crystalline material with significant birefringence is absented.

After analyzing the optical scheme with SVR [31], [32], and also taking into account the scheme for creating a radially polarized vector field by BPP together with QWP and HWP, described in Ref. [33], we propose our own scheme for creating a radially polarized vector field, which by introducing an additional HWP, the fast axis of which is oriented at 45° relative to the *x* axis direction, can be converted to azimuthally polarized.

2. Background

2.1 Schemes for Generating Radially and Azimuthally Polarized Vector Optical Fields

In contrast to the scheme used in Refs. [31], [32], as well as the scheme used in Ref. [33], to create a radially polarized vector field with a placed SVR, which is essentially equivalent to BPP, with a fast axis oriented in the *x* axis direction between two QWPs, the first axis of which is fast oriented at –45° direction relative to the *x* axis direction, and the second at 45° relative to the *x* axis direction (Fig. 1(a)).

The HWP with the orientation of the fast axis at 45° relative to the *x* axis direction allowed the radially polarized beam to be converted into azimuthally polarized (Fig. 1(b)). In order to illustrate the operation principle of SVR we described its work, based on the Jones matrices. Under the condition that the polarization angle of the incident light is 0° to the *x* axis direction, the Jones vector E_{in} of the incident light:

$$E_{in} = \begin{bmatrix} 1 \\ 0 \end{bmatrix}. \tag{3}$$

Since the fast axis of the QWP1 is oriented at the –45° to the *x* axis direction the Jones Matrix J_1 is expressed as:

$$J_1 = \frac{\sqrt{2}}{2} \begin{bmatrix} 1 & -i \\ -i & 1 \end{bmatrix}, \tag{4}$$

where *i* is the imaginary unit.

If the fast axis of the SVR is oriented at the x axis direction, the Jones matrix J_{SVR} is written as:

$$J_{SVR} = \exp\left(i\delta_1(x, y)\right)\begin{bmatrix} 1 & 0 \\ 0 & \exp\left(i\delta_2(x, y)\right) \end{bmatrix}. \tag{5}$$

Due to birefringent material used in the SVR plate, the phase delay between the ordinary and the extraordinary polarized light can be generating. In Eq. (5) $\delta_1(x, y)$ is the phase delay ordinary polarized light, and $\delta_2(x, y)$ is the phase delay between the ordinary and the extraordinary polarized light, $\delta_2(x, y)$ in general can have an arbitrary and continuous distribution, determined by the surface relief of the SVR.

The Jones matrix J_2 of the QWP2, whose fast axis is oriented at 45° to the x axis direction is given as:

$$J_2 = \frac{\sqrt{2}}{2}\begin{bmatrix} 1 & i \\ i & 1 \end{bmatrix}. \tag{6}$$

After passing the QWP1, the SVR and the QWP2, linearly polarized light is transformed to the radial polarized light in accordance with the SVR relief.

The Jones matrix J_3 of the HWP, whose fast axis is oriented at 45° to the x axis direction expressed as:

$$J_3 = \begin{bmatrix} 1 & 0 \\ 0 & i \end{bmatrix}. \tag{7}$$

The Jones matrix E_{out} of light passing through the QWP1, the SVR, the QWP2 is calculated as:

$$E_{out} = J_2 J_{SVR} J_1 E_{in} = \exp\left(i\delta_1(x, y) + i\delta_2(x, y)/2\right)\begin{bmatrix} \cos\left(\delta_2(x, y)/2\right) \\ \sin\left(\delta_2(x, y)/2\right) \end{bmatrix}. \tag{8}$$

The Jones matrix E_{out} of light passing through the QWP1, the SVR, the QWP2 and the HWP is expressed as:

$$E_{out} = J_3 J_2 J_{SVR} J_1 E_{in} = \exp\left(i\delta_1(x, y) + i\delta_2(x, y)/2\right)\begin{bmatrix} \sin\left(\delta_2(x, y)/2\right) \\ \cos\left(\delta_2(x, y)/2\right) \end{bmatrix}. \tag{9}$$

As can be seen from Eqs. (8) and (9), the polarization distribution of the output light is related to the amount of phase delay $\delta_2(x, y)$ is given the depth distribution of SVR relief.

The polarization distribution of the radial vector optical field can be defined as [33]:

$$E_{radial} = \begin{bmatrix} \cos\left(\theta(x, y)\right) \\ \sin\left(\theta(x, y)\right) \end{bmatrix}, \tag{10}$$

and the polarization distribution of azimuthal vector optical field can be defined as [34]:

$$E_{azimuthal} = \begin{bmatrix} \sin\left(\theta(x, y)\right) \\ \cos\left(\theta(x, y)\right) \end{bmatrix}. \tag{11}$$

Here $\theta(x, y)$ is the polarization angle of the linear polarized light at each point in the vector optical field. By comparing Eqs. (8) and (10) and also Eqs. (9) and (11) it is seen that $\theta(x, y)$ is related to $\delta_2(x, y)$ as follows:

$$\theta(x, y) = 2\delta_2(x, y). \tag{12}$$

The amount of phase delay $\delta_2(x, y)$ has following relationship with the depth distribution $h_{SVR}(x, y)$ of SVR plate:

$$h_{SVR}(x, y) = \frac{\lambda\delta_2(x, y)}{2\pi\left|n_o - n_e\right|}. \tag{13}$$

Considering Eq. (12) $h_{SVR}(x, y)$ can be written as:

$$h_{SVR}(x, y) = \frac{\lambda\theta(x, y)}{\pi|n_o - n_e|}. \tag{14}$$

From Eq. (14) the correspondence between the SVR and the depth distribution is visible. The continuity of the SVR depth variation will ensure the continuity of the polarization of the vector optical field. In the case of an SVR consisting of sectors, it is obvious that a larger number of sectors with a smaller depth step can provide a better picture of the continuity of the vector optical field. Distributions of radial and azimuthal optical fields in accordance with Eqs. (10) and (11), will take place at a continuous or close to continuous change in the relief of the depth of the SVR plate, in accordance with the expression:

$$h_{SVR}(x, y) = \frac{\lambda \arccos\left(x/\sqrt{x^2 + y^2}\right)}{\pi|n_o - n_e|}. \tag{15}$$

2.2 Choice of SVR Fabrication Technology

Recently, we have proposed a technology for fabrication OEs for various purposes on optical amorphous materials by the laser-induced microplasma (LIMP) etching [35], [36]. The essence of this technology can be summarized as follows. When scanning a focused laser beam with a wavelength $\lambda = 1.064\ \mu$m in the close contact of an optically transparent material and a highly absorbing solid target at the interface of two, a plasma flame is formed. A pressed graphite plate with a high absorption capacity of $A \sim 1.0$ in the wavelength range of 0.2 – 2.0 μm is used as a solid target. The emerging erosion plasma flame heats the back surface of the processed material to high temperatures, providing spallation ablation. Thus, the surface of the processed material is designed in accordance with the specified pattern and the required depth. The LIMP etching has your disadvantages and bottlenecks as all techniques of laser-induced plasma-assisted processing of transparent materials (for example, LIPAA [37], LIBWE [38], LIBDE [39] and etc). Several of ones are the use of laser beam absorber for initiation of plasma, the high influence of plasma parameters on the quality of surface processing [36], the low resolution in the plane of etching at the compared of photolithography, the additional removal of carbon-like products on the next step after laser writing of OEs [40]. However, such technology of fast fabrication of different OEs is very effective for scientific laboratories and small fabrications. The effectivity processing of transparent materials (with amorphous and crystalline structure) by LIMP was studied in the past [35], [36], [41]. This technology was successfully used to create a wide class of OEs [35] and recently it was tested in the fabrication of a random phase plate (RPP) on Iceland spar (uniaxial $CaCO_3$ crystal) plate [41]. In the experiments of the fabrication of RPPs (binary OEs), the range of laser irradiation regimes was determined, allowing to vary the etching depth in the range of up to 14 μm [41]. In this work we decided to try the use of LIMP for fabrication of SVR, which is a much more complex OE than RPP because of multilevel structure.

We would like to underline that the using a single OE consisting of segmented HWPs and allowing to receive azimuthally polarized light by simple turn the device from HWPs by 45° have advantages compared the alternative techniques. However, we also understood that the fabrication of OE with different orientations of the crystal axis of HWPs by LIMP technology is impossible, because it allows varying the etching depth, but does not allow changing the direction of the crystal axis in the corresponding sectors. In all the so-called schemes of single optical path (except for the scheme with segmented HWPs) for the conversion of linearly or circularly polarized light into radially or azimuthally polarized, except for the main element, which is a birefringent plate with a varying surface profile, additional polarization OEs are used as a rule. Therefore, we tried to construct our variants of schemes with a minimum number of OEs.

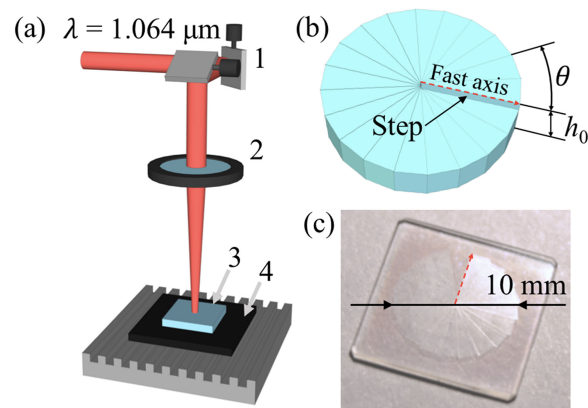

Fig. 2. SVR: (a) concept of SVR; (b) experimental setup for SVR's fabrication; (c) photo of the fabricated SVR.

3. SVR Fabrication Procedure

Experimental setup for the fabrication of SVR (Fig. 2(a)) contained a nanosecond fiber ytterbium laser ($\lambda = 1.064$ μm), whose beam was moved along the *x* and *y* axes by scanning system (1) based on galvanometric scanners. The focusing of the laser beam in the plane of the contact plate of Iceland spar (3) and solid carbon target (4) was carried out using a flat field objective ($f =$ 210 mm) (2), creating a beam diameter in the waist $d_0 = 50$ μm and processing in the field of 100 $\times$ 100 mm size.

To test the ability of our proposed schemes for obtaining a radially polarized vector optical field and an azimuthally polarized vector optical field, we chose the number of sectors for making an SVR equal to 20. Such a choice of the number of sectors was made by us on the basis of ideas that, with a small difference in the depth of the sectors, it would be possible to consider the surface relief SVR as continuous. In addition, when choosing the number of sectors, we were guided by a well-known fact, that with an increase in the number of sectors in SVR, the efficiency of converting linearly polarized light into light with radial polarization increases, approaching the theoretical limit. In the LIMP technology, the most important limitation on the number of sectors in the SVR is the diameter of the waist of the laser beam in the plane of contact between the plate and the solid target. With the beam waist diameter $d_0 = 50$ μm, implemented on an experimental setup, shown in Fig. 2(a), the number of sectors can reach theoretically ~600. However, even increasing the number of sectors to 100 will allow to consider the SVR profile continuous. Recent experiments on fabrication of SVR with a flat field objective, which creates a 25 μm focal spot in the scanning plane, definitely show that such increase of sectors' number to 100 or more is possible.

Estimation of etching depth for each of the SVR sectors, which schematic image is shown in Fig. 2(b), was performed according to Eq. (2). Calculation for $\lambda = 632.8$ nm, $n_o = 1.655$ and $n_e = 1.485$ (Table 1) showed that even with the number of sectors equal to 20, we fit into the experimentally found depth range.

Choosing the range of technological regimes ensuring the absence of cracks and punctures in the SVR sectors required a significant number of experiments. In such experiments we changed some laser irradiation parameters as the average power *P*, pulse repetition rate ν, scanning speed *U*, and the number of scans *N*. The pulse duration τ during the experiment was constant and equal to 50 ns. Experimental definitions of the range of regimes are given in Table 2. Depth of formed microrelief depends on the number of laser pulses $k = d_0\nu/U$, as shown in Fig. 3(a). On graphs presented the results with use of optimal pulses number in the laser spot of the single track for one and several scans. The higher accuracy of the desired depth was obtained at the less number pulses in the laser spot of single track (less than 5) and more numbers of scans (10 and more). At this case, the probability of crystalline sample damage was minimum. The maximum practical value

TABLE 1
SVR Etching Depth

Sector	Calculated *h*, µm	Measured *h*, µm	Relative deviation, %	Sector	Calculated *h*, µm	Measured *h*, µm	Relative deviation, %
1	0	0	0	11	3.722	3.730	0.2
2	0.372	0.375	0.8	12	4.094	4.101	0.2
3	0.744	0.750	0.8	13	4.467	4.475	0.2
4	1.117	1.121	0.4	14	4.839	4.830	0.2
5	1.489	1.494	0.3	15	5.211	5.221	0.2
6	1.861	1.857	0.2	16	5.584	5.593	0.2
7	2.233	2.239	0.3	17	5.956	5.967	0.2
8	2.606	2.617	0.4	18	6.328	6.337	0.1
9	2.978	2.986	0.3	19	6.700	6.712	0.2
10	3.350	3.345	0.1	20	7.072	7.086	0.1

TABLE 2
SVR Fabrication Regimes

Power density *q*, MW/cm²	Pulse duration τ, ns	Repetition rate ν, kHz	Scan speed *U*, mm/s	Number of scans *N*
7.64 – 22.01	50	50 – 80	700 – 800	1 – 10

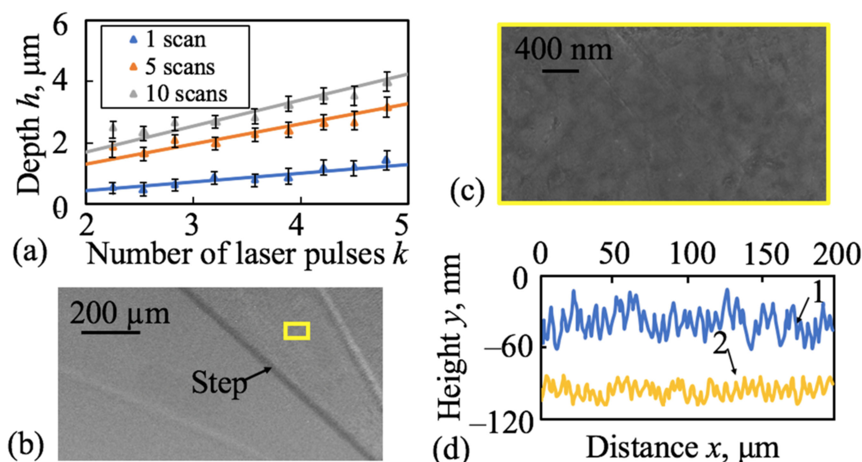

Fig. 3. SVR fabrication results: (a) the dependence of the $CaCO_3$ etching depth on the laser irradiation parameters for a different number of passes of the scanning system; (b, c) SEM images made of the fabricated SVR with different magnification; (d) roughness profiles of SVR sector after action of LIMP (curve 1) and after additional heat treatment (curve 2).

of number scans was about 15. The effectivity of etching greatly decreased at the more numbers of scans and the depth was practically not increased. Increase the number of laser pulses allowed to rise of processing effectivity at the phase optical elements fabrication. In this case, the more etching depth was achieved after one scan. However, a lot of pulses number raised probability of cracks and gouges formation in the treatment region. The optimal number of pulses was 3 – 5 for average power density and 2 – 3 for maximum power density from Table 2. The optimal ratio of pulse number and number of scans was determined experimentally. The study of crystalline materials

processing by this technique and its features presented in our previous work [41]. The fabrication of RPP on the $CaCO_3$ plate by LIMP technology and its testing in experimental setup of laser beam homogenization were successfully implemented, too. Also it can be seen that the range of $CaCO_3$ processing regimes is significantly narrower than the range of suitable regimes for processing of fused silica – an amorphous material [41]. We associate this fact with the significant birefringence of Iceland spar and its fragility (hardness on a scale Mohs is 3). The SVR fabricated by LIMP is shown in Fig. 2(c).

After fabrication procedure of SVR, it was studied with scanning electron microscope (SEM) «Zeiss Supra 40 VP» and profilometer «Hommel Tester T8000» with resolution of 10 nm. Figs. 3(b) and 3(c) shows SEM-image of the SVR's region, Fig. 3(d) shows roughness one of SVR's sectors. The spiral form of whole SVR and the gradually changing height of each sector are clearly seen from Figs. 3(b) and 3(c). The surface quality in the area of microplasma's flame action has been found acceptable. Also, there are no any punctures and cracks. The roughness R_z of the SVR's surface does not exceed 50 nm (Fig 3(d), curve 1). Measured etched depth of SVR and its relative deviation from calculated depth are given in Table 1. The table shows that relative error of etched depth of each sector of SVR decreases with the increasing depth of sectors and is no more than 0.8%. The decrease in the surface roughness values R_z of the SVR's sectors should lead to a further decrease in the relative error of etching depths in the sectors creating a deviation in the phase delay, and, accordingly, to an increase in the quality of the beam conversion. As far as we know, data on the annealing parameters of an anisotropic $CaCO_3$ crystal to reduce values R_z are not available in the literature. However, it was determined that when heated to a temperature of 1158 K at a normal atmospheric pressure of 1013 hPa $CaCO_3$ decompose into CaO and CO_2 without melting [42]. The regime of annealing the $CaCO_3$ plate with SVR was found experimentally. In Fig. 3(d) (curve 2) shows the roughness profile of one of the SVR's sectors after heat treatment in a furnace at a temperature of 823 ± 50 K for 12.0 ± 0.5 hours. The value of roughness R_z of surface of SVR sectors as a result of additional heat treatment was reduced to 35 ± 5 nm. This will be correct for any OEs fabricated by the LIMP technology on $CaCO_3$ plate.

During the experiments to determine the fabrication regimes of SVR on a $CaCO_3$ crystal, which is much more fragile than crystalline quartz, we found that the LIMP technology can also be used to form structures on the surface of other optically transparent crystalline materials with significant birefringence. However, it is obvious that for each specific material it will be necessary to select technological regimes that provide not only acceptable quality in the area of processing to a given etching depth, but also the absence of cracks and gouges surrounding the OEs formation area.

Also, we would like to note that there are no restrictions on the use of various scanning trajectories when creating relief on the SVR surface by the LIMP. The fact that in this paper we focused on the formation of a relief, which provides the creation of a radially polarized vector field and, accordingly, an azimuthally polarized vector field, achieving by simple placing HWP behind the block with SVR, in no way limits the use of this technology to create OEs, providing an arbitrary vector field.

4. SVR Testing Procedure

To confirm the ability of SVR fabricated by LIMP to generate radially or azimuthally polarized light such SVR was placed into experimental setup, which is shown in Fig. 4(a). The experimental setup for testing SVR was contained He-Ne laser ($\lambda = 632.8$ nm) (1), telescope with 3^x magnification (2) for beam expanding, polarizer (3), QWP1 (4), SVR (5), QWP2 (6), HWP (7) with the possibility of extraction from the optical system, analyzer (8), collecting lens (9) with focal length $f = 60$ mm, CMOS-camera «Gentec Beamage 3.0» (10), placed in the focal plane of the collecting lens. Choosing the He-Ne laser with beam quality $M^2 = 1.0$ in the experimental setup caused by minimizing errors related to the quality of conversion of linearly polarized Gaussian beams. It used at the testing procedure as the popular laser source with excellent/etalon parameters of beam (high coherence, beam quality and monochromaticity, small divergence, linear polarization, stability of optical power and other). The fiber laser had more optical power than He-Ne laser that allowed use fiber laser for SVR fabrication, but other parameters of this beam were a lot of worse than ones of He-Ne laser.

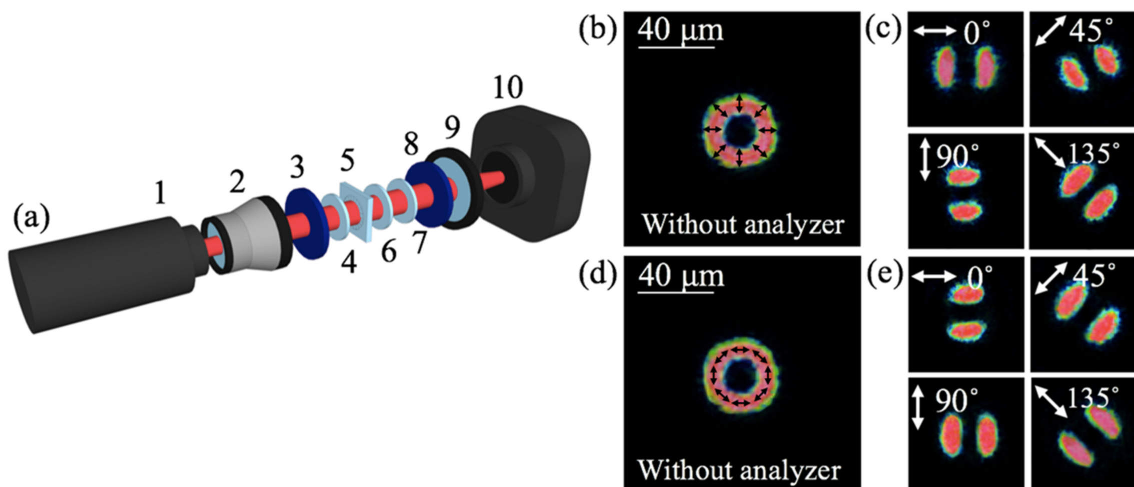

Fig. 4. Results of SVR testing: (a) experimental setup; (b, d) the ring-shaped intensity distribution of radially and azimuthally polarized beams in the far field; (c, e) the far field intensity distribution radially and azimuthally polarized beams upon analyzer rotation.

The demonstration of conversion the polarization light from linearly into radially was made through a registration of intensity distribution in the far field. The radius of wave front curvature here is close to infinity. Experimental far field intensity distribution was obtained in the focal plane after focusing of output beam by a spherical lens with focal length of 60 mm (Fig. 4(a)). The photosensitive area of the CMOS-camera was located in this plane. Registration was upon four positions of analyzer (0°, 45°, 90°, 135°) relative to the transmission axis of polarizer, also with its absence in the optical scheme. When the analyzer is absent in the SVR optical scheme, annular intensity distribution is observed in the lens focal plane (Fig. 4(b)). After placing the analyzer into the optical scheme, two rotating lobs during rotation of the analyzer are clearly seen (Fig. 4(c)). The analyzer blocked the light with linear polarization, which vector was perpendicular oriented to it axis. On the other hand, the light with linear polarization was transmitted if its vector was parallel oriented to analyzer axis. White arrows are the transmission axis direction of the analyzer. The obtained results show the evidence about the SVR placed between two orthogonally oriented QWPs convert of linearly polarized He-Ne laser beam into high quality radially polarized beam [15], [31].

The demonstration of conversion the polarization light from linearly into azimuthally was made through a registration of intensity distribution in the far-field after placement of the HWP, whose fast axis was oriented at 45° to the x axis direction, behind the SVR system. The registration was in the lens' focal plane upon four positions of analyzer (0°, 45°, 90°, 135°) relative to the transmission axis of polarizer, also with its absence in the optical setup. Obtained results (Figs. 4(d) and 4(e)) show that the SVR in conjunction with two QWPs and HWP is capable of converting a linearly polarized beam into a high quality azimuthally polarized beam.

The operating principle of SVR can be extended to the laser beams with other wavelengths. For effective work of SVR the etching depth should be recalculated by Eq. (2). Nowadays, experiments are being carried out on the application of SVR system for the transformation of a linearly polarized Gaussian beam of the Nd:YAG laser ($\lambda = 1.064\ \mu$m) with the nanosecond range of the pulse duration into radially or azimuthally polarized light. The SVR fabricated on the $CaCO_3$ plate is an excellent alternative to liquid crystal technologies for the high-power laser beams and ultra-short laser pulses with a high repetition rate, because the damage threshold of a transparent crystal plate is a higher than for liquid crystal elements. Moreover, the thermal stability of calcite reaches 1090 K that much higher than for liquid crystal [43].

4. Conclusion

To sum up, the following can be stated: a simple, reliable and efficient fabrication technology of SVR for conversion of linearly polarized Gaussian beams into radially or azimuthally polarized beams is presented. The SVR was produced on the plate of uniaxial crystal material (Iceland spar) the crystal axis of which is oriented parallel to the surface of the plate (Y-cut). The duration of fabrication of SVR with 20 sectors does not exceed 7 minutes.

Determination of laser irradiation ranges of regimes to achieve 50 nm roughness in the processed region and necessary depths of each sectors for perfect operation of SVR were found experimentally. It was experimentally shown that the roughness value R_z of the surface of the SVR sectors can be reduced to 35 ± 5 nm as a result of additional heat treatment in a furnace at a temperature of 823 ± 50 K for 12 ± 0.5 hours. The LIMP technology for SVR fabrication allows reaching a range of depths on $CaCO_3$ up to 14 μm.

During experiments on the formation of the SVR surface, it was found that necessary for the operation of the SVR the depth of its relief can be achieved by using different scanning trajectories. This fact leads to increases its application fields for processing of crystal plates for other purposes, which includes producing OEs, generating arbitrary vector optical fields. This follows from Eqs. (8) and (9) in which the distribution of phase delay $\delta_2(x, y)$, defined by the SVR relief depth distribution, can be made arbitrary.

SVR testing was performed with a He-Ne laser setup. Obtained test results provide our hope that SVR system will be widely applicated for conversion of linearly polarized Gaussian beams into radially and azimuthally polarized annular beams.

References

[1] S. Roy, K. Ushakova, Q. Van den Berg, S. Pereira, and H. Urbach, “Radially polarized light for detection and nanolocalization of dielectric particles on a planar substrate,” *Phys. Rev. Lett.*, vol. 114, no. 10, Mar. 2015, Art. no. 103903.
[2] Q. Zhan, “Trapping metallic Rayleigh particles with radial polarization,” *Opt. Exp.*, vol. 12, no. 15, pp. 3377–3382, 2004.
[3] G. Li, P. Zhang, and T. Zhang, “Three-dimensional cooling of a single atom by a pair of counter-propagating tightly focused beams,” *Opt. Exp.*, vol. 23, no. 18, pp. 23571–23581, Sep. 2015.
[4] Y. Kozawa and S. Sato, “Numerical analysis of resolution enhancement in laser scanning microscopy using a radially polarized beam,” *Opt. Exp.*, vol. 23, no. 3, pp. 2076–2084, Feb. 2015.
[5] K. Moh, X.-C. Yuan, J. Bu, S. Zhu, and B. Z. Gao, “Surface plasmon resonance imaging of cell-substrate contacts with radially polarized beams,” *Opt. Exp.*, vol. 16, no. 25, pp. 20734–20741, Dec. 2008.
[6] S. Quabis, R. Dorn, M. Eberler, O. Glockl, and G. Leuchs, “Focusing light to a tighter spot,” *Opt. Commun.*, vol. 179, no. 1/6, pp. 1–7, May 2000.
[7] M. Meier, V. Romano, and T. Feurer, “Material processing with pulsed radially and azimuthally polarized laser radiation,” *Appl. Phys. A*, vol. 86, no. 3, pp. 329–334, Jan. 2007.
[8] S. Matsusaka, Y. Kozawa, and S. Sato, “Micro-hole drilling by tightly focused vector beams,” *Opt. Lett.*, vol. 43, no. 7, pp. 1542–1545, Apr. 2018.
[9] M. Kraus, M. A. Ahmed, A. Michalowski, A. Voss, R. Weber, and T. Graf, “Microdrilling in steel using ultrashort pulsed laser beams with radial and azimuthal polarization,” *Opt. Exp.*, vol. 18, no. 21, pp. 22305–22313, Oct. 2010.
[10] V. Niziev and A. Nesterov, “Influence of beam polarization on laser cutting efficiency,” *J. Phys. D Appl. Phys.*, vol. 32, no. 13, pp. 1455–1461, Jul. 1999.
[11] C. Hnatovsky, V. G. Shvedov, and W. Krolikowski, “The role of light-induced nanostructures in femtosecond laser micromachining with vector and scalar pulses,” *Opt. Exp.*, vol. 21, no. 10, pp. 12651–12656, May 2013.
[12] Y. Kozawa and S. Sato, “Generation of a radially polarized laser beam by use of a conical Brewster prism,” *Opt. Lett.*, vol. 30, no. 22, pp. 3063–3065, Nov. 2005.
[13] R. Oron, S. Blit, N. Davidson, A. A. Friesem, Z. Bomzon, and E. Hasman, “The formation of laser beams with pure azimuthal or radial polarization,” *Appl. Phys. Lett.*, vol. 77, no. 21, pp. 3322–3324, Nov. 2000.
[14] J.-F. Bisson, J. Li, K. Ueda, and Y. Senatsky, “Radially polarized ring and arc beams of a neodymium laser with an intra-cavity axicon,” *Opt. Exp.*, vol. 14, no. 8, pp. 3304–3311, 2006.
[15] G. Machavariani, Y. Lumer, I. Moshe, A. Meir, and S. Jackel, “Spatially-variable retardation plate for efficient generation of radially- and azimuthally-polarized beams,” *Opt. Commun.*, vol. 281, no. 4, pp. 732–738, Feb. 2008.
[16] J. Xin, K. Dai, L. Zhong, Q. Na, and C. Gao, “Generation of optical vortices by using spiral phase plates made of polarization dependent devices,” *Opt. Lett.*, vol. 39, no. 7, pp. 1984–1987, Apr. 2014.
[17] G. M. Lerman and U. Levy, “Generation of a radially polarized light beam using space-variant subwavelength gratings at 1064 nm,” *Opt. Lett.*, vol. 33, no. 23, pp. 2782–2784, Dec. 2008.
[18] J. Xin, X. Lou, Z. Zhou, M. Dong, and L. Zhu, “Generation of polarization vortex beams by segmented quarter-wave plates,” *Chin. Opt. Lett.*, vol. 14, no. 7, Jul. 2016, Art. no. 070501.

[19] M. Beresna, M. Gecevicius, P. G. Kazansky, and T. Gertus, “Radially polarized optical vortex converter created by femtosecond laser nanostructuring of glass,” *Appl. Phys. Lett.*, vol. 98, no. 20, May 2011, Art. no. 201101.
[20] S. Fedotov *et al.*, “Direct writing of birefringent elements by ultrafast laser nanostructuring in multicomponent glass,” *Appl. Phys. Lett.*, vol. 108, no. 7, Feb. 2016, Art. no. 071905.
[21] M. Bashkansky, D. Park, and F. K. Fatemi, “Azimuthally and radially polarized light with a nematic SLM,” *Opt. Exp.*, vol. 18, no. 1, pp. 212–217, Jan. 2010.
[22] I. Moreno, M. M. Sanchez-Lopez, K. Badham, J. A. Davis, and D. M. Cottrell, “Generation of integer and fractional vector beams with q-plates encoded onto a spatial light modulator,” *Opt. Lett.*, vol. 41, no. 6, pp. 1305–1308, Mar. 2016.
[23] X. Yi *et al.*, “Generation of cylindrical vector vortex beams by two cascaded metasurfaces,” *Opt. Exp.*, vol. 22, no. 14, pp. 17207–17215, Jul. 2014.
[24] C.-H. Niu, B.-Y. Gu, B.-Z. Dong, and Y. Zhang, “A new method for generating axially-symmetric and radially-polarized beams,” *J. Phys. D Appl. Phys.*, vol. 38, no. 6, pp. 827–832, Mar. 2005.
[25] K. Moh, X.-C. Yuan, J. Bu, R. Burge, and B. Z. Gao, “Generating radial or azimuthal polarization by axial sampling of circularly polarized vortex beams,” *Appl. Opt.*, vol. 46, no. 30, pp. 7544–7551, Oct. 2007.
[26] B. Lim, P. Phua, W. Lai, and M. Hong, “Fast switchable electro-optic radial polarization retarder,” *Opt. Lett.*, vol. 33, no. 9, pp. 950–952, May 2008.
[27] T. Wang, S. Fu, S. Zhang, C. Gao, and F. He, “A Sagnac-like interferometer for the generation of vector beams,” *Appl. Phys. B*, vol. 122, no. 9, Sep. 2016, Art. no. 231.
[28] S. C. Tidwell, G. H. Kim, and W. D. Kimura, “Efficient radially polarized laser beam generation with a double interferometer,” *Appl. Opt.*, vol. 32, no. 27, pp. 5222–5229, Sep. 1993.
[29] F. Yue, D. Wen, J. Xin, B. D. Gerardot, J. Li, and X. Chen, “Vector vortex beam generation with a single plasmonic metasurface,” *ACS Photon.*, vol. 3, no. 9, pp. 1558–1563, Sep. 2016.
[30] F. Zhang *et al.*, “Efficient generation and tight focusing of radially polarized beam from linearly polarized beam with all-dielectric metasurface,” *Opt. Exp.*, vol. 24, no. 6, pp. 6656–6664, Mar. 2016.
[31] P. Phua *et al.*, “Mimicking optical activity for generating radially polarized light,” *Opt. Lett.*, vol. 32, no. 4, pp. 376–378, Feb. 2007.
[32] W. Lai, B. Lim, P. Phua, K. Tiaw, H. Teo, and M. Hong, “Generation of radially polarized beam with a segmented spiral varying retarder,” *Opt. Exp.*, vol. 16, no. 20, pp. 15694–15699, Sep. 2008.
[33] J. Wang *et al.*, “Vector optical field generation based on birefringent phase plate,” *Opt. Exp.*, vol. 25, no. 11, pp. 12531–12540, May 2017.
[34] O. Allegre, W. Perrie, S. Edwardson, G. Dearden, and K. Watkins, “Laser microprocessing of steel with radially and azimuthally polarized femtosecond vortex pulses,” *J. Opt.*, vol. 14, no. 8, Aug. 2012, Art. no. 085601.
[35] G. Kostyuk, M. Sergeev, R. Zakoldaev, and E. Yakovlev, “Fast microstructuring of silica glasses surface by NIR laser radiation,” *Opt. Lasers Eng.*, vol. 68, pp. 16–24, May 2015.
[36] V. P. Veiko *et al.*, “Laser-induced microplasma as a tool for microstructuring transparent media,” *Quantum Electron.*, vol. 47, no. 9, pp. 842–848, Sep. 2017.
[37] Y. Hanada *et al.*, “Development of practical system for laser-induced plasma-assisted ablation (LIPAA) for micromachining of glass materials,” *Appl. Phys. A*, vol. 79, no. 4-6, pp. 1001–1003, Sep. 2004.
[38] R. Böhme, A. Braun, and K. Zimmer, “Backside etching of UV-transparent materials at the interface to liquids,” *Appl. Surf. Sci.*, vol. 186, no. 1/4, pp. 276–281, Jan. 2002.
[39] B. Hopp, C. Vass, T. Smausz, and Z. Bor, “Production of submicrometre fused silica gratings using laser-induced backside dry etching technique,” *J. Phys. D Appl. Phys.*, vol. 39, no. 22, pp. 4843–4847, Nov. 2006.
[40] V. Koval, M. Sergeev, R. Zakoldaev, and G. Kostyuk, “Changes in the spectral characteristics of quartz-glass plates when they are processed with laser-induced plasma,” *J. Opt. Technol.*, vol. 84, no. 7, pp. 447–452, Jul. 2017.
[41] V. Shkuratova, V. Rymkevich, G. Kostyuk, and M. Sergeev, “Laser-induced microplasma as effective tool for phase elements fabrication on amorphous and crystalline materials,” *J. Laser Micro Nanoeng.*, vol. 13, no. 3, pp. 211–215, Dec. 2018.
[42] R. S. Mikhail, S. Hanafi, S. Abo-el-Enein, R. Good, and J. Irani, “Morphology and surface area changes in the thermal dissociation of Iceland spar,” *J. Colloid Interface Sci.*, vol. 75, no. 1, pp. 74–84, May 1980.
[43] Z. Cao, L. Xian, L. Hu, X. Lu, and Q. Mu, “Temperature effect on the diffraction efficiency of the liquid crystal spatial light modulator,” *Opt. Commun.*, vol. 267, no. 1, pp. 69–73, Nov. 2006.